Construction and Building Materials 110 (2016) 369–380

Contents lists available at ScienceDirect

Construction and Building Materials

journal homepage: www.elsevier.com/locate/conbuildmat

Combined effect of carbonation and chloride ingress in concrete

Xingji Zhu [a], Goangseup Zi [a,*], Zhifeng Cao [b], Xudong Cheng [b]

[a] School of Civil, Environmental & Architectural Engineering, Korea University, 5 Ga 1, An-Am Dong, Sung-Buk Gu, Seoul 136-701, Republic of Korea
[b] College of Pipeline and Civil Engineering, China University of Petroleum (Huadong), No. 66 Changjiang West Road, Qingdao, Shandong Province, China

HIGHLIGHTS

- A comprehensive model for the combined carbonation and chloride ingress in concrete is developed.
- The effect of CSH is directly considered for the estimation of the degree of carbonation.
- The changes of the pore structure and the binding capacity are considered for the combined action.
- The corrosion initiation can be accelerated significantly by the combined mechanism.

ARTICLE INFO

Article history:
Received 26 August 2015
Received in revised form 8 October 2015
Accepted 12 February 2016
Available online 22 February 2016

Keywords:
Depassivation of reinforcement
Numerical modeling
Carbonation of concrete
Chloride penetration
Combined action
Pore structure change

ABSTRACT

The combined effect of carbonation and chloride ingress in concrete is studied in this paper. Based on the change of the pore structure and the chemical equilibrium, a comprehensive model is proposed for this problem. A coupled simulation of the transports of carbon dioxide, chloride ions, heat and moisture is carried out. Several sets of experimental data were compared with the prediction by the numerical model developed in this paper, for its verification. Parametric study shows that the differences between the combined mechanism and the independent mechanisms are significant in many aspects.

1. Introduction

The corrosion of reinforcement due to the penetration of chloride ions and the carbonation of concrete is an important problem which reduces the durability of reinforced concrete structures. Once the chloride concentration around the surface of the steel reinforcement exceeds a certain threshold concentration, or the pH value of the concrete pore solution decreases to a threshold value due to carbonation reaction, the steel reinforcement will undergo the so-called depassivation process [1–3]. With the intrusion of oxygen, electrochemical reactions occur generating corrosion products on the surface of the steel reinforcement. This results in cracking of the concrete cover due to the swelling pressure of the corrosion products [4,5]. Of course, the cross sectional area of the reinforcement decreases because of the corrosion mechanisms. Therefore, it is important to develop a tool to predict the depassivation mechanisms of steel reinforcement accurately for durability design and pre-planning and maintenance of RC structures. The time-dependent load capacity of a reinforced concrete structure should be assessed by taking into account the growth of the corrosion layer within the cross section of the reinforcements. This subject is certainly important to study, and possible to incorporate. However, we focus only on the initiation of the corrosion in this combined mechanism in this paper.

The transport of chloride ions causing the depassivation of steel reinforcement in concrete is well studied and a number of models are available for the simulation of the process [1,6–11]. Some of them studied the influence of initial cracks in concrete [12–15] and the effect of loading on chloride transport [16,17]. In the literature [18–20], numerical modeling of the entire process of concrete corrosion damage was proposed, in which physical and electrochemical model can be coupled with cracking mechanical model. The corrosion of reinforcement caused solely by chloride ingress has been sufficiently studied and is well understood.

The ingress of chloride ions is often significant in a marine atmospheric environment, where the supply of chloride ions due to salt spray and the carbonation of concrete can occur simultaneously [21]. For instance, the entrances of cross-harbour tunnels are subjected to severe salt spray conditions, and at the same time

* Corresponding author.
E-mail address: g-zi@korea.ac.kr (G. Zi).

http://dx.doi.org/10.1016/j.conbuildmat.2016.02.034
0950-0618/

Nomenclature

B_T heat transfer coefficient of concrete surface
B_c chloride transfer coefficient of concrete surface
B_h humidity transfer coefficient of concrete surface
$C_{CO_2,b}$ molar concentration of carbon dioxide on concrete surface
C_{CO_2} molar concentration of carbon dioxide in the gas phase of pore
C_{CSH} molar concentration of the calcium silicate hydrate (CSH) in concrete
C_{bc} content of bound chloride
$C_{ch,d}$ and $C_{ch,s}$ molar concentration of dissolved and solid $Ca(OH)_2$, respectively
$C_{fc,b}$ chloride concentration on concrete surface
$C_{fc,env}$ chloride concentration of the surrounding environment
C_{fc} content of free chloride
C_{tc} content of total chloride
C_{th} threshold chloride content of non-carbonated concrete
C_{th}^{car} threshold chloride content considering the influence of carbonation
$D_{CO_2}^{car}$ diffusion coefficient of carbon dioxide in concrete
D_{fc} chloride diffusion coefficient of non-carbonated concrete
D_{fc}^{car} diffusion coefficient of chloride considering the influence of carbonation
D_h^{car} diffusion coefficient of moisture considering the influence of carbonation
FA ratio of cement replacement by fly ash
I_h internal source of heat
I_{CSH} rate of consumption of carbon dioxide due to the reaction with CSH
I_{ch} rate of consumption of carbon dioxide due to the reaction with dissolved $Ca(OH)_2$
I_d dissolved rate of solid $Ca(OH)_2$
I_{rc} source term reflecting the release of the free chloride ions from the Friedel's salt due to carbonation
I_{w_e} pore water generated by carbonation reaction
$M(\cdot)$ molar mass of the substance given in the round brackets
P_{CO_2} volume fraction of carbon dioxide in the environment
T_b temperature of concrete surface
T_{env} temperature of the surrounding environment
$[C_{CSH}]_0$ initial molar concentration of the CSH in concrete
$[C_{CaO}]_0$ initial molar concentration of the total calcium oxide in concrete
$[C_{ch,d}]_0$ initial molar concentration of the dissolved calcium hydroxide before carbonation
ΔV_{ch} and ΔV_{CSH} molar volume change of $Ca(OH)_2$ and CSH after reacting with CO_2, respectively
$\Delta\phi_c$ ultimate reduction of the porosity after carbonation
Ω tortuosity of concrete
Ω_0 initial tortuosity of concrete
α_L and β_L parameters for Langmuir isotherm
α_c degree of carbonation
$\alpha_{L,c}$ α_L parameter for Langmuir isotherm corrected for carbonation
δ constrictivity of concrete
δ_0 initial constrictivity of concrete
κ correction factor of vapor phase water generated by carbonation
λ thermal conductivity
$\boldsymbol{J}_{CO_2}$ flux of carbon dioxide
$\boldsymbol{J}_{ch,d}$ flux of hydroxide ions
$\boldsymbol{J}_{fc,b}$ flux of chloride ions on concrete surface
$\boldsymbol{J}_{fc}$ flux of free chloride ions
$\boldsymbol{J}_{h,b}$ flux of humidity through the concrete surface
$\boldsymbol{q}_b$ heat flux through the concrete surface
$\bar{r}_p$ dimensionless size of peak radius
$\bar{r}_{p,0}$ dimensionless parameter of peak radius before carbonation
$\bar{r}_{p,c}$ dimensionless parameter of peak radius after carbonation
ϕ current porosity of concrete
ϕ_0 porosity of non-carbonated concrete
ϕ_{hc} porosity of hardened binder
ϕ_{w_e} volume fraction of evaporable pore water
ρ_{CO_2} gas density of carbon dioxide
a/b and w/b aggregate-to-binder ratio and water-to-binder ratio
b binder content per unit volume of concrete
c_q specific heat
d reduction factor of the binding capacity of chloride ions due to carbonation
$f_c(w/b)$ and $f_c(FA)$ influence functions of water-to-binder ratio and fly ash replacement ratio on the change of peak radius due to carbonation
$f_h(w/b)$ influence function of water-to-binder ratio on estimating the peak radius size of non-carbonated concrete
$f_p(\Omega,\delta)$ influence function of the change of the pore structure on the diffusion coefficients of chloride ions and moisture
h_b relative humidity of concrete surface
h_{env} relative humidity of the surrounding environment
r_{CSH} reaction rate of CSH with carbon dioxide
$r_{p,ref}$ reference size of peak radius
r_p size of peak radius in different degrees of carbonation

they must withstand carbon dioxide pollution with a concentration five to six times higher than that in most other on-shore environments. A similar concern may be made for structures in modern cities at those latitudes where de-icing salts are heavily used in winter, and where the concentration of carbon dioxide is high because of pollution and traffic. Given the interaction of carbonation with the durability threat caused by the chloride ions ingress, both factors must be taken into account in the development of a simulation tool.

Carbonation influences the transport of chloride ions in concrete significantly. Numerous experiments have been carried out to study this influence [22–31]. According to those experimental researches, the precise influence of carbonation is so complicated that it is difficult to note whether carbonation will accelerate or decelerate the durability damage due to chloride ions. The influence of carbonation on the diffusion coefficient of chloride ions depends on the types and mix proportions of concretes considered experimentally [22,29–31].

An interesting phenomenon was reported in a new type of test where carbonation and chloride ingress were loaded alternately [24–26]. In that alternating test, the concentration of chloride ions was maximum near to the front of carbonation. Although carbonation and chloride ingress take place simultaneously, it should be noted that the diffusion of chloride ions is much faster than the rate of carbonation. That is, before carbonation, concrete usually contains Friedel's salt due to the chloride ion bound inside of concrete. Once the Friedel's salt reacts with carbon dioxide during the carbonation process, chloride ions are released to the pore solution in concrete as shown in the following equation.

$$3CaO\cdot Al_2O_3\cdot CaCl_2\cdot 10H_2O + 3CO_2 \rightarrow 3CaCO_3 + 2Al(OH)_3 + CaCl_2 + 7H_2O \quad (1)$$

These released chloride ions increase the free chloride concentration significantly higher than that in a simple diffusion of chloride ions from the surface to the inside. Therefore, in order to analyze and predict the combined effects of carbonation and chloride ingress, it is essential to model realistically how carbonation interacts with chloride transport without carbonation.

Some works proposed direct influence functions of carbonation on chloride transport in concrete [28,32] but they analyzed merely the influence of carbonation on the chloride diffusion coefficient. Those models cannot explain the results from the alternating tests [24,25]. A number of simulations of the carbonation process are found in the literature [33–35]. The carbonation process consists of the diffusion of carbon dioxide and the reaction of carbon dioxide with calcium hydroxide. In most of the works, the influence of other hydrate products, such as calcium silicate hydrate $3CaO \cdot 2SiO_2 \cdot 3H_2O$ (CSH), is hardly considered in the simulation of the carbonation process. We build a comprehensive model for the combined effect of carbonation and chloride ingress which will be verified with experimental data.

After this introduction in Section 1, the mathematical expression of our model for this combined problem is given in Section 2. The influence mechanism of carbonation to chloride transport is also given in this section. The boundary conditions and the solving method of the numerical model are shown in Section 3. The numerical results are compared with the experimental data in Section 4 to verify the model. A parametric study on this numerical model is given in Section 5. The conclusion for this work follows in Section 6.

2. Model of carbonation and chloride transport

2.1. Process of the carbonation

The carbonation of concrete is a complex physical and chemical process. In our model, this process is divided into four parts: (1) transport of carbon dioxide, (2) mass balance of dissolved calcium hydroxide, (3) dissolution of solid calcium hydroxide into concrete pore solution and (4) chemical reaction of CSH with carbon dioxide. The governing equations can be given by

$$\frac{\partial(\phi-\phi_{w_e})C_{CO_2}}{\partial t}+\nabla\cdot\boldsymbol{J}_{CO_2}=-I_{ch}-I_{CSH} \tag{2}$$

$$\frac{\partial\phi_{w_e}C_{ch,d}}{\partial t}+\nabla\cdot\boldsymbol{J}_{ch,d}=-I_{ch}+I_d \tag{3}$$

$$\frac{\partial C_{ch,s}}{\partial t}=-I_d \tag{4}$$

$$\frac{\partial C_{CSH}}{\partial t}=-r_{CSH} \tag{5}$$

where C_{CO_2} is the molar concentration of carbon dioxide in the gas phase of the pores (mol/m^3 of pore air), ϕ is the current concrete porosity, ϕ_{w_e} is the volume fraction of evaporable pore water (m^3 solution/m^3 concrete), $\boldsymbol{J}_{CO_2}$ is the flux of carbon dioxide, I_{ch} and I_{CSH} is the rate of the carbon dioxide consumption due to its chemical reaction with $Ca(OH)_2$ and CSH, respectively, $C_{ch,d}$ is the molar concentration of the dissolved calcium hydroxide (mol/m^3 of solution), $\boldsymbol{J}_{ch,d}$ is the flux of hydroxide ions, I_d is the dissolved rate of the solid calcium hydroxide to the pore water, $C_{ch,s}$ is the molar concentration of solid calcium hydroxide (mol/m^3 of concrete), C_{CSH} is the molar concentration of CSH in concrete (mol/m^3 of concrete), r_{CSH} is the reaction rate of CSH with carbon dioxide. The right hand sides in Eqs. (2)–(5) are determined by Papadakis et al.'s carbonation model [36–38]. Those are summarized in Appendix A. The relation between ϕ_{w_e} and h can be estimated according to the BSB model [39] as given in Appendix B.

A number of estimation methods for the diffusion coefficient of carbon dioxide $D^{car}_{CO_2}$ are available in literature [34,38,40]. The following simple formula is adopted in this study:

$$D^{car}_{CO_2}=1.64\times10^{-6}\phi_{hc}^{1.8}(1-h)^{2.2} \tag{6}$$

where ϕ_{hc} is the porosity of hardened binder paste and h is the humidity. Note that ϕ_{hc} is a function of porosity [38]. During the process of carbonation, the influence of the porosity change on the diffusion coefficient of carbon dioxide should be considered.

Some of the unhydrated silicates contained in concrete, such as $3CaO \cdot SiO_2$ (C_3S) and $2CaO \cdot SiO_2$ (C_2S), can react with carbon dioxide, too. However, the amounts of C_3S and C_2S are small and difficult to determine accurately. Their rate of the chemical reaction with carbon dioxide is close to the reaction rate of CSH. They are all insensitive to the degree of carbonation [36]. Therefore, we take C_3S and C_2S into the content of CSH C_{CSH} to reflect the content of total solid carbonatable constituents of hardened binder paste in concrete for simplicity.

The pH value of concrete can be estimated by the concentration of the dissolved calcium hydroxide [36,41].

$$\mathrm{pH}=\begin{cases}14+\log(2\times10^{-3}C_{ch,d}) & \text{for } C_{ch,d}\geqslant1\times10^{-3}\\ 8.3 & \text{otherwise}\end{cases} \tag{7}$$

Actually, the low bound of pH value for a completely carbonized concrete also depends on the concentration of CO_2 from the environment [4]. Since the ultimate limit of pH would be far below the threshold value which causes depassivation of the reinforcement, the dependence of the ultimate value in Eq. (7) is not considered in this model.

Conventionally, the degree of carbonation is estimated by the consumption of only the dissolved calcium hydroxide [34]. However, the carbon dioxide also reacts with solid constituents of the hardened binder. This changes the pore structure and influences the migration of ions. Therefore the reactions of CSH and other unhydrated silicates during carbonation process also needs to be considered in the degree of carbonation. Here, the degree of carbonation α_c is defined as:

$$\alpha_c=1-\frac{C_{ch,s}+\phi_{w_e}C_{ch,d}+3C_{CSH}}{[C_{CaO}]_0} \tag{8}$$

where $[C_{CaO}]_0$ is the initial molar concentration of the total calcium oxide in concrete. This value can be estimated approximately by using the mix proportions of concrete [42].

2.2. Change of pore structure due to carbonation

When carbonation occurs, the pore structure and material properties of concrete will also change [29,38,43,44]. This will seriously affect the transport of moisture, chloride ions and carbon dioxide. Therefore, establishing a mathematical model which can reflect the variations of concrete pore structure in different degrees of carbonation is important. Here, we consider the change of the porosity and the peak radius size of capillary pores [13,45].

The porosity ϕ in different carbonation degrees can be given by

$$\phi=\phi_0-\Delta\phi_c\ \alpha_c \tag{9}$$

where ϕ_0 is the porosity of non-carbonated concrete and $\Delta\phi_c$ is the ultimate reduction of the porosity when the concrete is fully carbonated. $\Delta\phi_c$ can be estimated by [38]

$$\Delta\phi_c=\left([C_{CaO}]_0-3[C_{CSH}]_0\right)\Delta V_{ch}+[C_{CSH}]_0\Delta V_{CSH} \tag{10}$$

where $[C_{CSH}]_0$ is the initial molar concentration of the CSH in concrete, and $\Delta V_{ch} = 3.85 \times 10^{-6}$ m^3/mol and $\Delta V_{CSH} = 15.39 \times 10^{-6}$ m^3/mol are the molar volume changes of calcium hydroxide and CSH after they react with carbon dioxide, respectively. $[C_{CSH}]_0$ can be given by

$$[C_{CSH}]_0 = \frac{P_{CSH}[C_{CaO}]_0}{3} \tag{11}$$

where P_{CSH} is the molar proportion of calcium oxide in the form of CSH and can be estimated approximately based on the formulae given in the literature [46].

The peak radius of capillary pores reflects the connectivity of pore structure which influences the mobility of chloride ions in concrete [13,45]. It can be calculated based on the pore size distribution which may be obtained by the mercury intrusion porosimetry. The change of the peak radius size due to carbonation is significant, especially for fly ash concretes [43]. Some of previous studies about the influence of carbonation on the pore size distribution are summarized in the literature [47].

Here, for simplicity, we assume that the size of peak radius is linearly proportional to the degree of carbonation α_c. Then the size of peak radius r_p in different degrees of carbonation can be given by

$$r_p = 5 \times 10^{-8} r_{p,ref}\left[(\bar{r}_{p,c} - \bar{r}_{p,0})\alpha_c + \bar{r}_{p,0}\right] \tag{12}$$

where $r_{p,ref} = 1$ m is a reference size and $\bar{r}_{p,0}$ and $\bar{r}_{p,c}$ are dimensionless parameters of peak radius before and after carbonation. $\bar{r}_{p,0}$ and $\bar{r}_{p,c}$ depend on the water-to-binder ratio and the fly ash content, i.e.

$$\bar{r}_{p,0} = f_h(w/b) \tag{13}$$

$$\bar{r}_{p,c} = f_h(w/b)\, f_c(w/b)\, f_c(FA) \tag{14}$$

where $f_h(w/b)$ is the influence of the water-to-binder ratio on estimating the peak radius size of non-carbonated concrete and $f_c(w/b)$ and $f_c(FA)$ are the influence functions of the water-to-binder ratio and fly ash replacement ratio on the change of the peak radius due to carbonation. These three functions determined by experimental data [38,43,47–55] are as follows:

$$f_h(w/b) = -4.66(w/b)^2 + 8.72(w/b) - 1.78 \quad \text{for } 0.3 \leqslant w/b \leqslant 0.55 \tag{15}$$

$$f_c(w/b) = 10.59(w/b)^2 - 11.36(w/b) + 4.29 \quad \text{for } 0.3 \leqslant w/b \leqslant 0.55 \tag{16}$$

$$f_c(FA) = 5.38FA^2 + 12.92FA + 1 \quad \text{for } 0 \leqslant FA \leqslant 30\% \tag{17}$$

where FA is the ratio of cement replacement by fly ash.

It is shown in Fig. 1 the change of the peak radius for ordinary Portland cement and fly ash concretes before and after carbonation in different water-to-binder ratios and fly ash contents. The change of the peak radius by carbonation is marginal in the case of ordinary Portland cement concretes, as shown in Fig. 1a. Fly ash concretes are often considered more durable because of relatively low porosity. However, it is found in Fig. 1b that the increase of the peak radius by carbonation is so significant in the case of fly ash concretes. The peak radius becomes almost three times greater than the initial value after carbonation with 20% of fly ash. Similar results were reported in the literature [47,56]; a coarser capillary pore structure was formed in the process of carbonation for furnace slag concretes.

2.3. Influence of carbonation on the initiation of chloride-induced corrosion

2.3.1. Transport of chloride ions with carbonation

We assume that transport of the chloride ions equation after carbonation still meets Fick's second law of diffusion. The total amount of chloride in a unit volume of concrete consists of the free chloride in the pore solution and the bound chloride (Friedel's salt), i.e.

$$C_{tc} = \phi_{w_e} C_{fc} + C_{bc} \tag{18}$$

where C_{tc} is the content of total chloride in a unit volume of concrete (mol/m^3 of concrete) and C_{fc} is the content of free chloride ions (mol/m^3 of pore solution). C_{bc} is the content of bound chloride (mol/m^3 of concrete). A part of the bound chloride can participate in the chemical reaction shown in Eq. (1) and release free chloride ions.

The amount of the bound chloride depends on the concentration of the free chloride in the pore solution as well as the degree of the carbonation because we consider the carbonation. Therefore, the instantaneous rate of the total chloride can be expressed as

$$\frac{\partial C_{tc}}{\partial t} = \frac{\partial \phi_{w_e} C_{fc}}{\partial t} + \frac{\partial C_{bc}}{\partial C_{fc}}\frac{\partial C_{fc}}{\partial t} + \frac{\partial C_{bc}}{\partial \alpha_c}\frac{\partial \alpha_c}{\partial t} \tag{19}$$

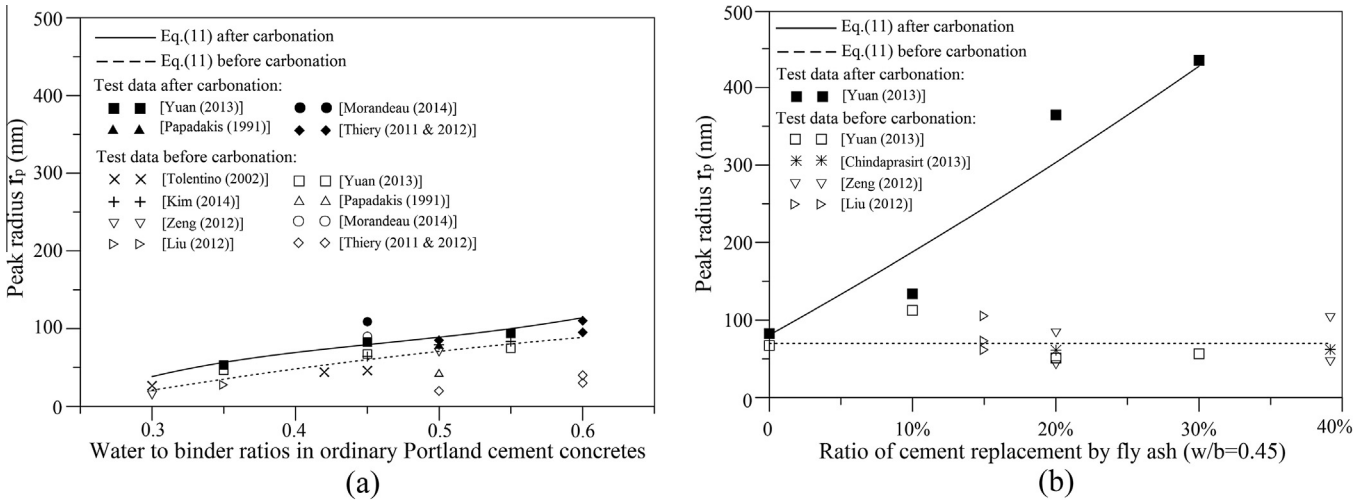

Fig. 1. Change of peak radius depending on (a) w/b and (b) fly ash content [38,43,47–55].

where, $\partial C_{bc}/\partial C_{fc}$ is an isotherm between bound chloride and free chloride. $\partial C_{bc}/\partial \alpha_c$ also can be described by an isotherm in which the carbonation should be considered.

The governing equation considering the convective term is given by

$$\frac{\partial C_{tc}}{\partial t} = \nabla \cdot D_{fc}^{car} \nabla \phi_{w_e} C_{fc} + \nabla \cdot D_h^{car} \phi_{w_e} C_{fc} \nabla h \tag{20}$$

where D_{fc}^{car} and D_h^{car} are the diffusion coefficients of free chloride ions and moisture depending on the degree of carbonation.

By inserting Eq. (19) into Eq. (20), then the governing equation can be arranged as

$$\frac{\partial \phi_{w_e} C_{fc}}{\partial t} + \frac{\partial C_{bc}}{\partial C_{fc}} \frac{\partial C_{fc}}{\partial t} + \frac{\partial C_{bc}}{\partial \alpha_c} \frac{\partial \alpha_c}{\partial t} = \nabla \cdot D_{fc}^{car} \nabla \phi_{w_e} C_{fc} + \nabla \cdot D_h^{car} \phi_{w_e} C_{fc} \nabla h \tag{21}$$

Eq. (22) can be simplified further into

$$\frac{\partial \phi_{w_e} C_{fc}}{\partial t} + \nabla \cdot \boldsymbol{J}_{fc} = I_{rc} \tag{22}$$

where $\boldsymbol{J}_{fc}$ is the flux of chloride ions and I_{rc} is the source term reflecting free chloride ions released from the Friedel's salt due to carbonation. They can be given by

$$\boldsymbol{J}_{fc} = -\frac{1}{1 + \frac{1}{\phi_{w_e}} \frac{\partial C_{bc}}{\partial C_{fc}}} \left(D_{fc}^{car} \nabla \phi_{w_e} C_{fc} + \phi_{w_e} C_{fc} D_h^{car} \nabla h \right) \tag{23}$$

$$I_{rc} = -\frac{1}{1 + \frac{1}{\phi_{w_e}} \frac{\partial C_{bc}}{\partial C_{fc}}} \frac{\partial C_{bc}}{\partial \alpha_c} \frac{\partial \alpha_c}{\partial t} \tag{24}$$

The binding capacity of non-carbonated concrete is often defined by the slope of a binding isotherm [57,58]. Here, we use the Langmuir isotherm model in which

$$C_{bc} = \frac{\alpha_L \phi_{w_e} C_{fc}}{1 + \beta_L M(Cl^-) \phi_{w_e} (C_{fc}/b)} \tag{25}$$

where $M(\cdot)$ molar mass of the substance given in $(\cdot)$ (kg/mol), b is the binder content per unit volume of concrete. Note that $M(Cl^-)$ and b are introduced to match the units. α_L and β_L are parameters to be determined by the type of concrete [13,58]. As suggested in the literature [13], we take $\beta_L = 4.0$. Based on experimental data, for ordinary Portland and fly ash concrete, parameter α_L is considered as a quadratic function of the fly ash replacement ratio FA, i.e.

$$\alpha_L = -15.5FA^2 + 1.8FA + 11.8 \quad \text{for } 0 \leqslant FA \leqslant 0.4 \tag{26}$$

The binding capacity of concrete must also be influenced by carbonation. It was reported that the residual binding capacity is reduced to less than 20% of the initial capacity after carbonation [21,24,25]. The chloride binding capacity of concrete before and after carbonation are shown in Fig. 2. To compare data from different sources [13,21,24,25], the binding capacity is divided by α_L. Based on these experimental studies, we suggest replacing α_L in Eq. (25) by $\alpha_{L,c} = 0.12\alpha_L$ for the concrete after complete carbonation. For simplicity, a linear dependency is assumed to incorporate this influence in the binding capacity of concrete. Then, Eq. (25) is modified as

$$C_{bc} = \frac{\alpha_L (1 - d\alpha_c) \phi_{w_e} C_{fc}}{1 + \beta_L M(Cl^-) \phi_{w_e} (C_{fc}/b)} \tag{27}$$

where d is the reduction factor of chloride ion binding capacity due to carbonation. d is given by

$$d = 1 - \frac{\alpha_{L,c}}{\alpha_L} = 0.88 \tag{28}$$

Then, the change of the bound chloride content according to different free chloride concentration and carbonation degrees can be described as shown in Fig. 3.

The slope of the binding isotherm $\partial C_{bc}/\partial C_{fc}$ which reflects the residual binding capacity of the concrete in different degrees of carbonation is given by

$$\frac{\partial C_{bc}}{\partial C_{fc}} = \frac{\alpha_L (1 - d\alpha_c) \phi_{w_e} C_{fc}}{\left[1 + \beta_L M(Cl^-) \phi_{w_e} (C_{fc}/b)\right]^2} \tag{29}$$

And, the source term I_{rc} in Eq. (24) can be calculated as

$$I_{rc} = \frac{d\alpha_L \phi_{w_e} C_{fc} (I_{ch} + I_{CSH})}{\left(1 + \frac{1}{\phi_{w_e}} \frac{\partial C_{bc}}{\partial C_{fc}}\right) \left[1 + \beta_L M(Cl^-) \phi_{w_e} (C_{fc}/b)\right] [C_{CaO}]_0} \tag{30}$$

2.3.2. Influence of carbonation on the diffusion coefficient of chloride ions

The change of the pore structure due to carbonation is considered in the diffusion coefficients of chloride ions and moisture D_{fc}^{car} and D_h^{car}

$$D_{fc}^{car} = D_{fc} f_p(\Omega, \delta) \tag{31}$$

$$D_h^{car} = D_h f_p(\Omega, \delta) \tag{32}$$

where D_{fc} and D_h are the initial diffusion coefficients of the chloride and the moisture before carbonation and their specific calculations

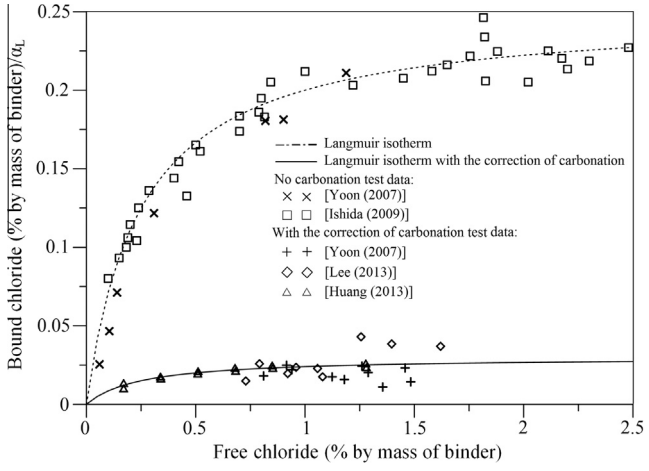

Fig. 2. Chloride binding capacity of concrete before and after carbonation.

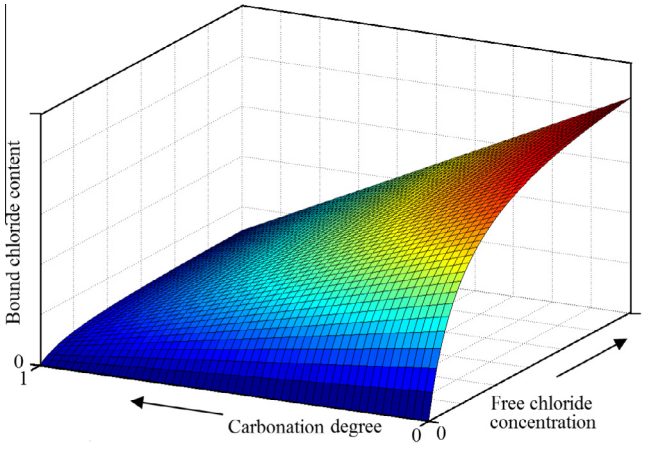

Fig. 3. Change of bound chloride content according to different free chloride concentrations and carbonation degrees.

are given in Appendices C and D according to the literature [44,59–62], respectively. $f_p(\Omega,\delta)$ is the influence of pore structure change to the diffusion coefficients. This influence can be characterized by tortuosity Ω and constrictivity δ of the pore structure, i.e.

$$f_p(\Omega,\delta)=\frac{\delta}{\delta_0}\frac{\Omega_0}{\Omega} \tag{33}$$

where δ_0 and Ω_0 are the concrete initial constrictivity and initial tortuosity, respectively. The tortuosity is a measure of how tortuous the pore channels are. This is typically given by a function of the porosity. The constrictivity measures how narrow pore channels for the transport of ions are. This can be defined by using the peak radius size r_p. The tortuosity and constrictivity may be given by the following equations [13,45]

$$\Omega=-b_1\tanh[b_2(\phi-b_3)]+b_4 \tag{34}$$

$$\delta=c_1\tanh[c_2(\log\bar{r}_p+c_3)]+c_4 \tag{35}$$

where b_1 to c_4 are parameters to be determined and $\bar{r}_p=r_p/r_{p,ref}$ is a dimensionless size of peak radius. $r_{p,ref}$ is introduced because of the unit problem. According to the literature [13,29,43,45], we take $b_1=1.5$, $b_2=8.0$, $b_3=0.25$, $b_4=2.5$, $c_1=0.395$, $c_2=4.0$, $c_3=5.95$ and $c_4=0.405$.

2.3.3. Change of threshold chloride content due to carbonation

The reduction of the threshold concentration due to carbonation causes the depassivation of the steel surface to be accelerated. According to the literature [4,63], the ratio of the concentration of the chloride ions to the concentration of hydroxide ions is constant at the critical state of the initiation of corrosion. Therefore, the threshold value for different degree of carbonation is given by

$$C_{th}^{car}=\frac{C_{ch,d}}{[C_{ch,d}]_0}C_{th} \tag{36}$$

where, $[C_{ch,d}]_0$ is the initial molar concentration of the dissolved calcium hydroxide before carbonation, C_{th} is the threshold chloride content of non-carbonated concrete. Note that the concentration of the dissolved calcium hydroxide $C_{ch,d}$ is a function of carbonation as shown in Eq. (3).

2.4. Transfer of heat and moisture

Because temperature and humidity take important roles in the foregoing analysis, the transport of heat and moisture must be considered in another form of conservation equations.

$$\rho c_q\frac{\partial T}{\partial t}-\lambda\nabla^2T=I_h \tag{37}$$

$$\frac{\partial\phi_{w_e}}{\partial h}\frac{\partial h}{\partial t}+\nabla\cdot\boldsymbol{J}_h=I_{w_e} \tag{38}$$

where T is the absolute temperature (K), ρ is the mass density of concrete (kg/m^3), c_q is the specific heat (W/Kkg), λ is the thermal conductivity (J/mK), I_h is the internal source of heat (W/m^3), $\partial w_e/\partial h$ is the moisture isotherm. $\boldsymbol{J}_h=-D_h^{car}\nabla h$ is the flux of moisture. I_{w_e} is the generation of water by the carbonation reaction of the dissolved calcium hydroxide with carbonic acid, which is given by

$$I_{w_e}=\frac{\kappa I_{ch}M(H_2O)}{\rho_w} \tag{39}$$

where κ is the correction factor for vapor phase water generated by carbonation, simply taken as 1.0 in this study. The reaction of CSH with carbon dioxide does not generate free water.

3. Boundary condition and model solving

The fluxes of the chloride ions, humidity and heat transport on the boundary are given by Eqs. (40)–(42) [44,59,64,65]:

$$\boldsymbol{J}_{fc,b}=B_c(C_{fc,b}-C_{fc,env})+C_{fc,env}J_{h,b} \tag{40}$$

$$\boldsymbol{J}_{h,b}=B_h(h_b-h_{env}) \tag{41}$$

$$\boldsymbol{q}_b=B_T(T_b-T_{env}) \tag{42}$$

where $\boldsymbol{J}_{fc,b}$ is the chloride flux to the concrete's surface (mol/m^2 s), B_c is the surface chloride transfer coefficient (m/s), $C_{fc,b}$ is the chloride concentration at the concrete surface (mol/m^3 of solution), $C_{fc,env}$ is the chloride concentration of the surrounding environment (mol/m^3 of solution), $\boldsymbol{J}_{h,b}$ is the flux of humidity through the concrete surface (m/s). B_h is the surface humidity transfer coefficient (m/s), h_b is the relative humidity in pores on the concrete surface, h_{env} is the relative humidity of the surrounding environment, $\boldsymbol{q}_b$ is the concrete heat flux (W/m^2), B_T is the heat transfer coefficient of concrete (W/m^2 K), T_b is the temperature at the concrete surface (K), T_{env} is the temperature of the surrounding environment (K).

In the actual project, carbon dioxide is generally in contact with concretes in the gaseous phase. Therefore, the concentration of carbon dioxide in the environment can be considered as the boundary condition for concrete carbonation. It can be obtained from the volume fraction of the carbon dioxide in the environment P_{CO_2}, i.e.

$$C_{CO_2,b}=\frac{P_{CO_2}\rho_{CO_2}}{M(CO_2)} \tag{43}$$

where $\rho_{CO_2}=1.977$ kg/m^3 is the gas density of carbon dioxide.

The foregoing governing equations were incorporated into a commercial finite element program, COMSOL. Using the function of Physics Builder provided by this software, a user-supplied submodule is developed for this model. Then, the spatial and temporal discretization can be completed by this software and the numerical model can be solved by its solver.

4. Verification of the model

4.1. Transport of chloride ions in completely carbonated concrete

A number of test data can be found for the transport of chloride ions after complete carbonation. However, most of them did not provide the information on the pore structure of concrete after carbonation. Yuan et al. carried out a series of experiments and provided enough information on the change of pore structure due to carbonation [29,43,66]. They used three different mix proportions of concrete for their experiment. They also reported the effect of fly ash. These concrete specimens were immersed in 5% NaCl solution at 35 °C for two months. The concentration of the chloride ions was measured with respect to the depth of specimens before and after

Table 1
Mix proportions and values of parameters used in the numerical model for completely carbonated concrete test.

Specimen	Mix proportions			Values of parameters				
	w/b	a/b	FA	D_{fc} (m^2/sec)	ϕ_0	$\Delta\phi_c$	$\bar{r}_{p,0}$	$\bar{r}_{p,c}$
A-1	0.35	3.9	0	3.8×10^{-12}	10.86	2.04	0.94	0.88
A-2	0.35	5.3	0	4.3×10^{-12}	11.59	4.06	1.35	1.65
A-3	0.35	6.7	0	6.5×10^{-12}	16.72	6.52	1.50	1.68
B-1	0.45	5.3	10	4.7×10^{-12}	12.03	3.81	2.45	2.58
B-2	0.45	5.3	20	3.7×10^{-12}	11.55	4.60	1.02	7.49
B-3	0.45	5.3	30	3.1×10^{-12}	10.37	2.11	1.13	8.70

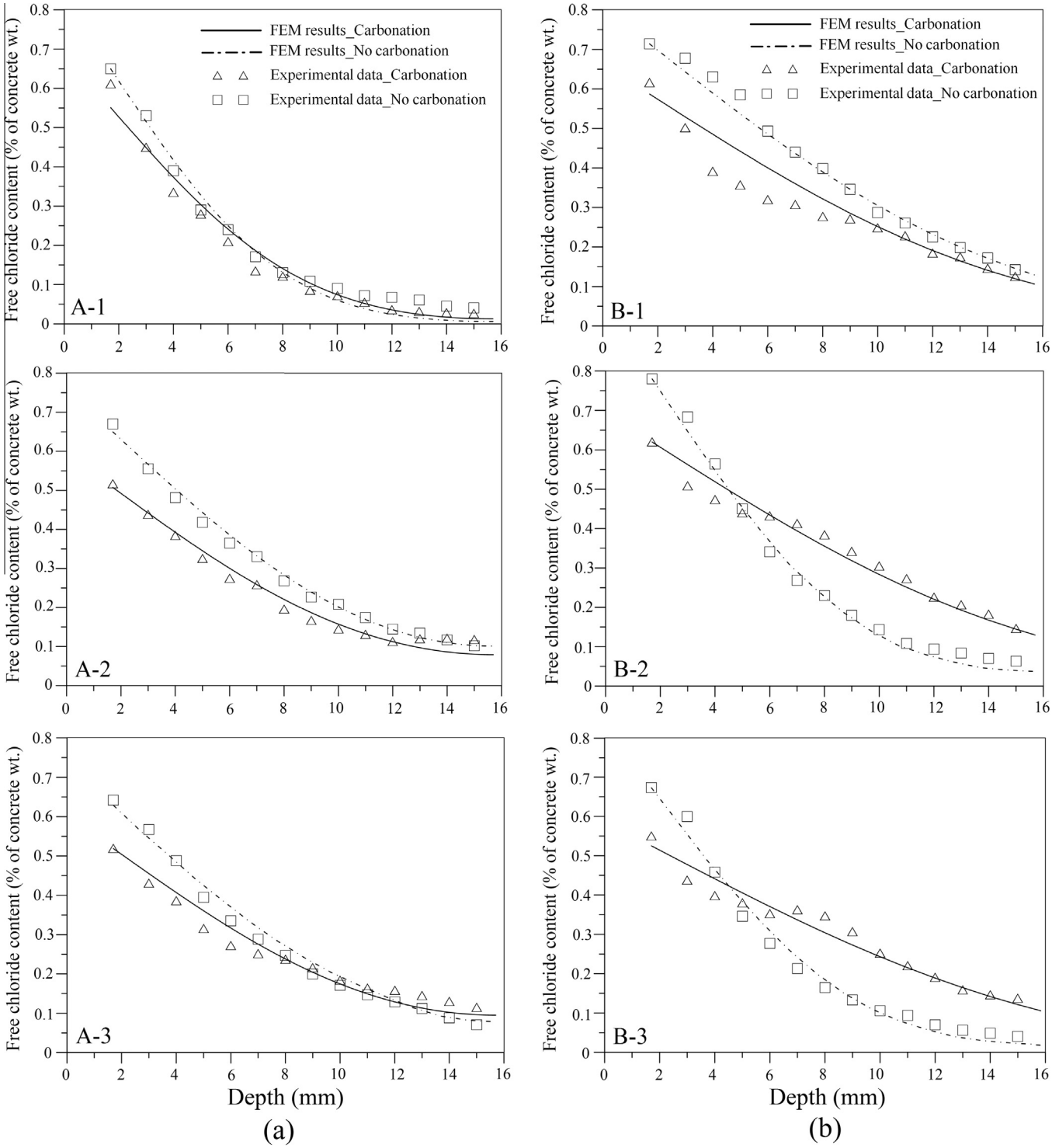

Fig. 4. Concentration of free chloride ions of different specimens before and after carbonation with respect to the depth of specimen; (a) ordinary Portland concretes A-1, A-2 and A-3 and (b) fly ash concretes B-1, B-2 and B-3 [29,43].

the carbonation. They also measured the change of porosity and the size of the peak radius by the mercury injection test. The mix proportions and the parameters used in the numerical model are given in Table 1. The chloride diffusion coefficients of non-carbonated concretes D_{fc} were calculated based the experimental data.

The concentration of the free chloride ions is plotted with respect to the depth of specimens in Fig. 4. It is found that the change of the microstructure due to carbonation is well captured in our numerical model. Fig. 4b shows that fly ash indeed reduces the diffusion coefficient of chloride ions. However, it also shows that carbonation accelerates the migration of chloride ions in the concrete with fly ash in the states of no carbonation. The effect of the fly ash replacement is also captured in the numerical model.

4.2. Alternating test of carbonation and chloride ion transport

In the alternating test, specimens are subjected to carbonation for a certain period of time, and then to penetration by chloride

Table 2
Mix proportions and parameters used in the alternating numerical model.

Specimen	Mix proportions			Values of parameters		
	w/b	a/b	FA	D_{fc} (m^2/sec)	$[C_{CaO}]_0$ (mol/m^3 of concrete)	P_{CSH} (%)
H5FA20	0.38	3.6	20	5.5×10^{-12}	3072	37.5
N5FA00	0.42	4.2	0	3.9×10^{-11}	3252	35.4
D-1	0.45	4.8	0	3.9×10^{-12}	3300	34.9
D-2	0.50	5.3	0	4.6×10^{-12}	2970	38.8
D-3	0.55	5.4	0	5.4×10^{-12}	2698	42.7

ions. These two tests are carried out alternately. Lee et al. tested four types of concrete, including high-strength and normal strength concretes, with different proportions of fly ash in the alternating test condition for more than fifty weeks [24]. The concrete specimens were immersed in 5% NaCl solution at 25 °C for one week, and then placed in a carbonation chamber with 10% of CO_2, 40 °C temperature and 60% of relative humidity for the following week. The mix proportions and the parameters used in the numerical model are given in Table 2. The values of other parameters can be determined by the equations given in this paper. The values of $[C_{CaO}]_0$ and P_{CSH} are estimated based on the empirical formulae given in the literature [42,46].

The numerical simulations of this combined action are shown in Figs. 5 and 6. The depths of the carbonation for fly ash and ordinary Portland normal concrete were 13.8 and 10.6 mm, respectively. Except these two specimens, the depth of carbonation was too small to investigate the combined action for other specimens in their test. It was found from their test that the carbonation process accelerated the transport of chloride ions significantly, and that the concentration of chloride ions is high near the front of the carbonation. These phenomena are captured well by the numerical model.

The chloride ions bound in the form of Friedel's salt are released to the pore solution in the process of carbonation, according to Eq. (1). The carbonation also reduces the binding capacity significantly, as modeled in Eq. (27). I.e., the release of chloride ions with less binding capacity increases the concentration of chloride ions near the front of the carbonation as shown in Figs. 5 and 6.

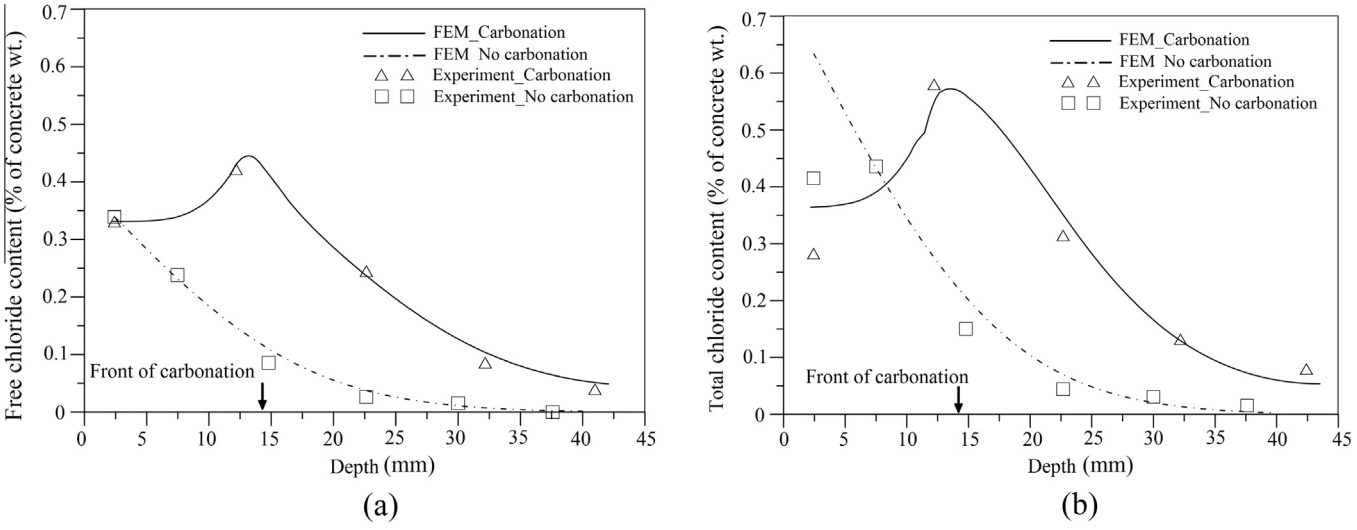

Fig. 5. Concentrations of (a) free and (b) total chloride ions with respect to the depth of specimen (H5FA20) made of a high strength concrete with 20% of fly ash replacement [24].

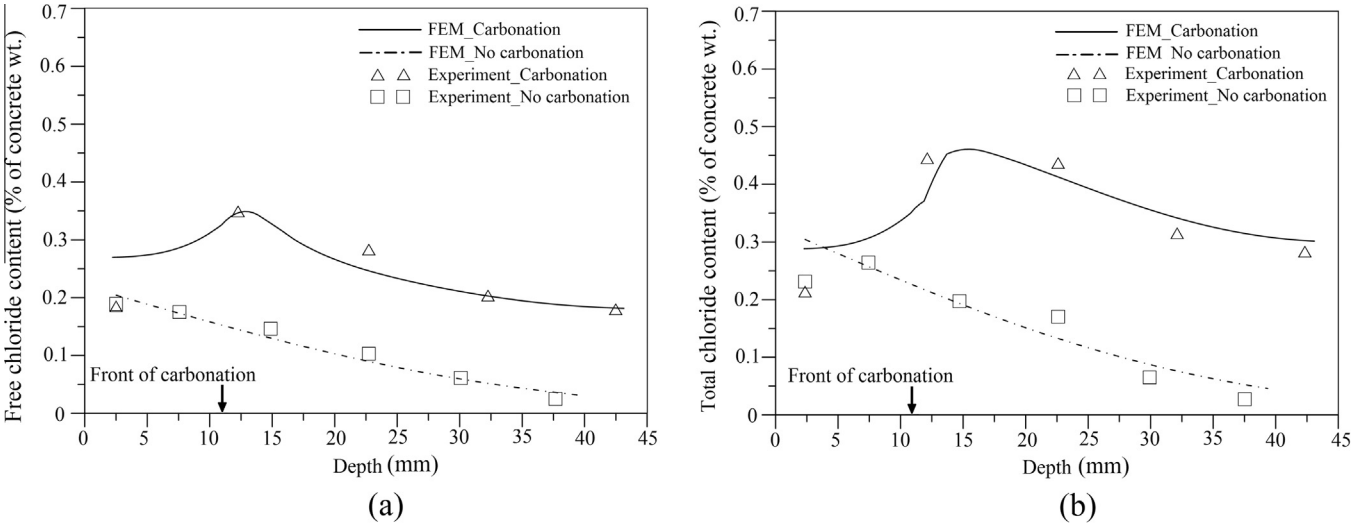

Fig. 6. Concentrations of (a) free and (b) total chloride ions with respect to the depth of specimen (N5FA00) made of a normal strength concrete without fly ash [24].

Yoon also carried out a similar test for three water-to-binder ratios [25]. He placed the specimens in a carbonation chamber with 5% of CO_2 and at 20 °C and with 65% of relative humidity for three days, and then immersed them in 0.5 M NaCl solution for the next three days. These two procedures were repeated until the test was finished. The mix proportions and the parameters used in the numerical model are also given in Table 2. The test data was compared with the numerical calculation in Fig. 7. A similar trend as in Lee et al.'s test was obtained. It is interesting to see a noticeable local increase of the total chloride ions. The location where the concentration of the total chloride ions is high is just beyond the front of the carbonation. Note that the binding capacity beyond the front of the carbonation is still high and this region is neighbored with the carbonated concrete in which the concentration of the chloride ions is high because of the ion release explained in Eq. (1).

5. Parametric study using the numerical model

5.1. Problem description

A part of fly ash concrete beam is taken to establish a two dimensional model for a parametric study. The cross section of the beam is 400 mm × 750 mm. The cover thickness is taken as 35 mm. The bottom surface is set as the boundary of temperature, humidity, carbon dioxide and chloride ions ingress. The top surface and both sides are set as the insulation border. The material properties of the concrete are as follows: aggregate-to-binder ratio $a/b = 6$, water-to-binder ratio $w/b = 0.4$, fly ash replacement ratio FA = 30%, molar proportion of calcium oxide in the forms of CSH in concrete p = 50%, reduction factor of chloride ion binding capacity due to carbonation d = 0.88, heat transfer coefficient $B_T = 7.75$ W/(m^2 K), surface chloride transfer coefficient $B_c = 1$ m/s, surface humidity transfer coefficient $B_h = 3 \times 10^{-7}$ m/sec, moisture reference diffusion coefficient $D_{h,ref} = 3 \times 10^{-10}$ m^2/sec, chloride reference diffusion coefficient $D_{fc,ref} = 5 \times 10^{-12}$ m^2/sec and equivalent diffusion coefficient of dissolved calcium hydroxide $D_{ch,d} = 1 \times 10^{-13}$ m^2/sec.

We use two trigonometric functions to express the variation of temperature and humidity. The maximum and minimum ambient temperatures are taken as 30 °C and −10 °C, respectively. The ambient humidity is taken as being between 0.7 and 0.8. The chloride concentration of the surrounding environment is taken as 25 kg/m^3 in solution. The beam is assumed to be under a normal atmospheric environment, that is, the volume fraction of carbon dioxide in air P_{CO_2} is equal to 0.03%.

5.2. Effect of fly ash content on chloride transport

In order to show the influence of carbonation on free chloride concentration clearly, we ignore the change of the reference diffusion coefficients of concretes with different fly ash contents in this parametric study. Although the water-to-binder ratio and the aggregate-to-binder ratio are also important, these effects are not considered in this paper because they have already been discussed in many literatures [36,41,60,64]. Fig. 8 shows the influence of carbonation on chloride ingress in concretes with different fly ash contents. We can find that a higher fly ash content has a more pronounced effect on the acceleration of chloride ions ingress.

5.3. Effect of carbon dioxide concentration on the penetration of chloride ions

Fig. 9 shows the influence of different carbon dioxide concentrations on the concrete surface. We can observe the influence of different carbonation depths on the distribution of the chloride

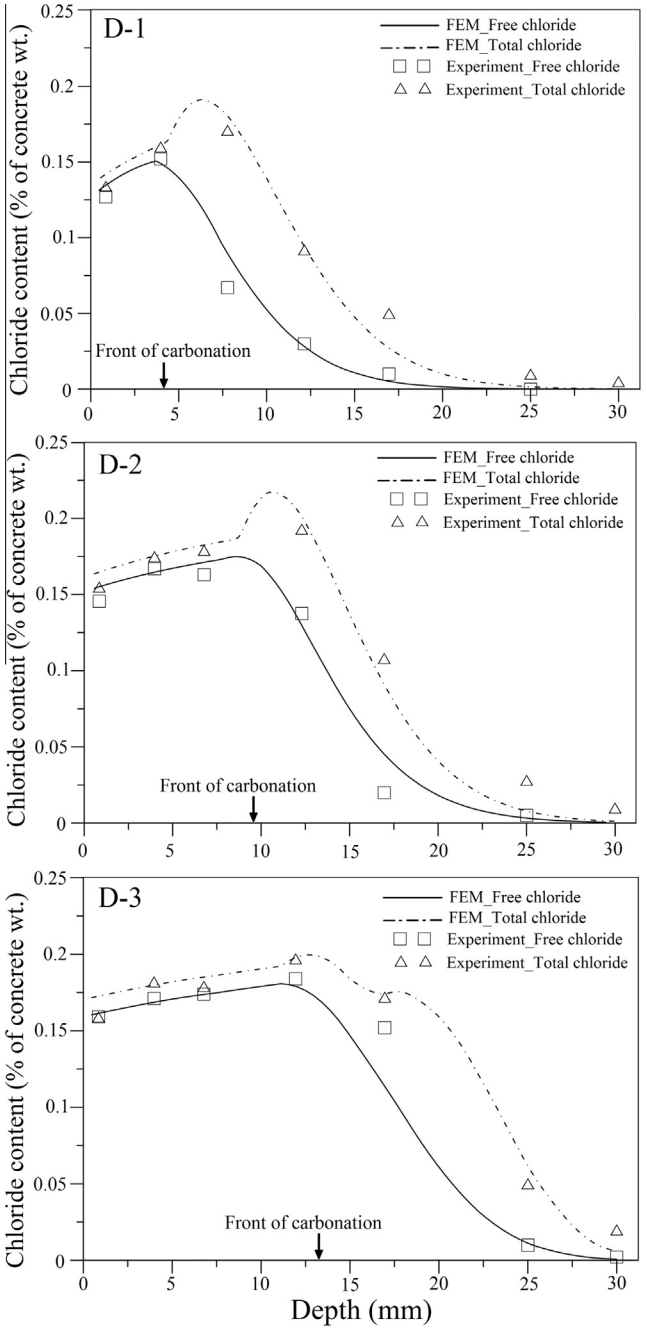

Fig. 7. Concentration of total and free chloride ions for different water-to-binder ratio under the combined action of carbonation and the transport of chloride ions.

ion concentration in concrete. In this case study, only the concentration of carbon dioxide on the boundary are adjusted to 0, 0.01%, 0.02%, 0.03% and 0.05%, respectively. All other parameters and boundary conditions are kept same. With the increase of the volume fraction of carbon dioxide, the concentration of the free chloride ions also increases significantly. The front of carbonation looks like a new boundary of chloride transport and the carbonation may be separated from this combined action.

5.4. Effect of carbonation on the initiation time of corrosion

Fig. 10 shows the influence of carbonation on the initiation time of corrosion in this case study. The chloride concentration and the corrosion threshold calculated in the placement of the

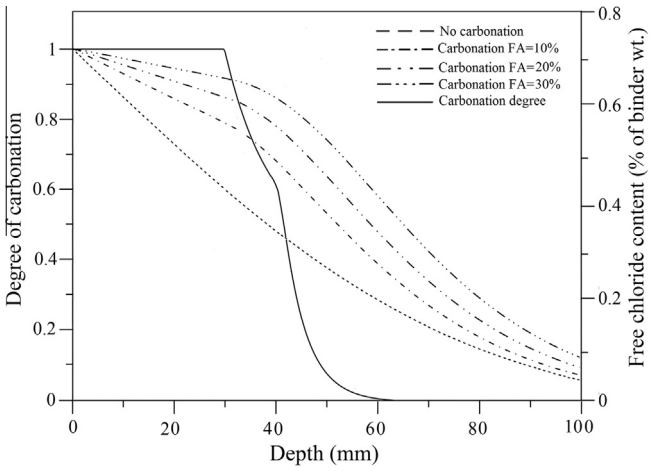

Fig. 8. Effect of fly ash replacement on free chloride content distribution according to different depths.

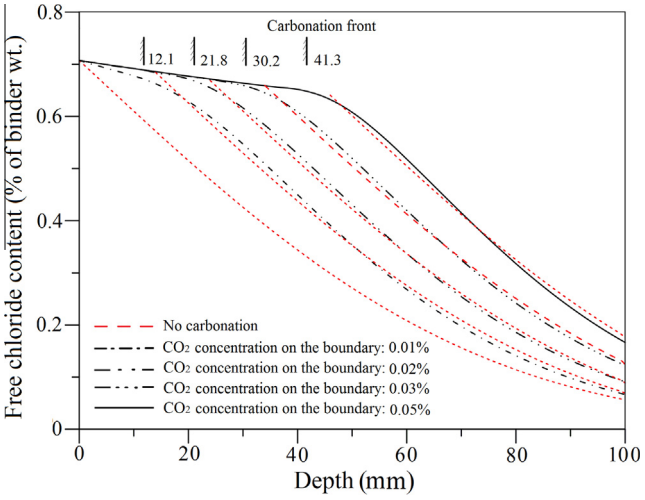

Fig. 9. Influence of carbon dioxide concentration on the surface to the distribution of chloride ion concentration in concrete after 50 years.

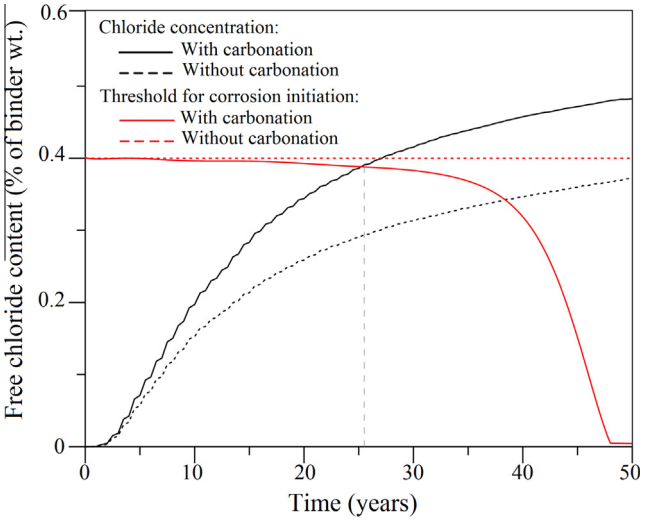

Fig. 10. Initiation time of corrosion.

reinforcement are shown in Fig. 10. By the definition, if the chloride concentration, C_{fc}, becomes equal to the threshold value, C_{th}^{car}, the corrosion of the reinforcement would be initiated. Due to the carbonation-induced change of pore structure and the binding capacity of chloride ions, the apparent diffusion coefficient of chloride ions in the carbonated zone increases by Eqs. (29) and (31). Meanwhile, the bound chloride ions are released to the pore solution during the process of carbonation, according to Eq. (1). These effects increase the concentration of free chloride ions. The process of carbonation consumes the dissolved calcium hydroxide, which reduces the threshold value as given in Eq. (36). In this illustrative example, this reinforced concrete section designed for 50 years service life would have the durability problem only less than 30 years later.

6. Conclusions

1. A comprehensive numerical model for the combined carbonation and chloride ingress is developed. The transport of carbon dioxide, chloride ions, heat and moisture are coupled in this model.
2. We propose a new method to calculate the degree of carbonation and pH value based on the chemical mechanism of carbonation. The reaction of carbon dioxide with calcium hydroxide and other hydration products, such as CSH, is considered in this method.
3. A set of empirical formulae for the change of peak radius size and porosity is proposed to consider the influence of carbonation on the change of pore structure.
4. The reduction of the chloride binding capacity of concrete is included in the numerical model. The Langmuir isotherm is modified to consider the effect of carbonation to the binding capacity.
5. Several sets of experimental data are compared with the prediction by the numerical model for its verification. The results support the validity of this model.
6. The numerical results show that, the initiation time of reinforcement corrosion is reduced significantly by this combined mechanism. In the example considered in this study, the initiation time of the reinforcement corrosion is reduced about 40%. And, a higher fly ash content causes a more pronounced effect on the carbonation-induced acceleration of chloride ion ingress.

Acknowledgment

This research was supported by a grant (15RDRP-B066780-03) from Regional Development Research Program funded by Ministry of Land, Infrastructure and Transport of Korean government. Xingji Zhu appreciates the support of the China Scholarship Council (CSC).

Appendix A. Mass exchange rate in the carbonation of concrete

According to the literature [36], the right hand sides of Eqs. (2)–(5) are given by

$$I_{ch} = \phi f_w r_c C_{CO_2} H(C_{ch,d}) \quad (A.1)$$

$$I_{CSH} = 3 r_{CSH} \quad (A.2)$$

$$r_{CSH} = a_c k_{CSH} V_{CSH} C_{CO_2} C_{CSH} \quad (A.3)$$

$$I_d = 0.5 \phi f_w V_{ch} k_{ch} a_c (C_{OH^-}^{eq} - C_{OH^-}) C_{ch,s} \quad (A.4)$$

where f_w is the volume fraction of the water film on the wall of pores, r_c is the dependence of the reaction on the temperature, $H(\cdot)$ is the Heaviside step function, a_c is the surface area of pores per unit of concrete volume, $k_{CSH} \simeq 1 \times 10^{-9}$ m/s is the rate constant for the reaction of CSH with CO_2, $V_{CSH} = 150 \times 10^{-6}$ m^3/mol is the molar volume of CSH. $V_{ch} = 3.37 \times 10^{-5}$ m^3/mol is the molar volume of solid $Ca(OH)_2$, $k_{ch} = 5 \times 10^{-5}$ m/s is the mass transfer coefficient for the dissolution of solid $Ca(OH)_2$, $C^{eq}_{OH^-} = 43.2$ mol/m^3 is the molar concentration of OH^- per unit volume of pore water at equilibrium, $C_{OH^-} = 2 \times C_{ch,d}$ is the molar concentration of OH^-.

Here, the temperature dependence of r_c is converted to an Arrhenius type equation, i.e.,

$$r_c = A_c \exp\left(\frac{E_c}{RT}\right) \tag{A.5}$$

where $A_c \simeq 359\,\text{sec}^{-1}$ is a scaling factor of the reaction, $E_c \simeq 442$ J/mol is the activation energy of the reaction [37], $R = 8.314$ J/(mol · K) is the universal gas constant and T is the absolute temperature.

Appendix B. Relation between ϕ_{w_e} and h

The relation between ϕ_{w_e} and h can be estimated as:

$$\phi_{w_e} = \frac{Ck_mV_mh}{(1-k_mh)[1+(C-1)]k_mh} \tag{B.1}$$

where, C, k_m and V_m are parameters. For $t_e \geqslant 5$ days and $0.3 \leqslant W/c \leqslant 0.7$, they can be determined as [67]

$$C = \exp(855/T) \tag{B.2}$$

$$k_m = \frac{C(1-1/n_w)-1}{C-1} \tag{B.3}$$

$$n_w = (2.5 + 15/t_e)(0.33 + 2.2w/b) \tag{B.4}$$

$$V_m = (0.068 - 0.22/t_e)(0.85 + 0.45w/b) \tag{B.5}$$

where t_e is the age of concrete hydration in days. The unit of temperature is K.

Appendix C. Chloride diffusion coefficient of non-carbonized concrete

The chloride diffusion coefficient of non-carbonated concrete D_{fc} can be given as

$$D_{fc} = D_{fc,ref}h_1(h)h_2(T)h_3(t_e) \tag{C.1}$$

where $D_{fc,ref}$ is the chloride reference diffusion coefficient (m^2/s) and $h_1(h), h_2(T)$ and $h_3(t_e)$ are the influence functions of pore relative humidity, temperature and age, respectively. They are given as

$$h_1(h) = \left[1 + \frac{(1-h)^4}{(1-h_c)^4}\right] \tag{C.2}$$

$$h_2(T) = \exp\left(\frac{U_c}{RT_{c,ref}} - \frac{U_c}{RT}\right) \tag{C.3}$$

$$h_3(t_e) = \left(\frac{t_{ref}}{t_e}\right)^m \tag{C.4}$$

where U_c is the activation energy of the chloride diffusion process, its value is between 32 and 44.6 kJ/(mol · K) for different w/b [60], $T_{c,ref}$ and t_{ref} are the reference temperature and time at which the reference chloride diffusivity $D_{fc,ref}$ has been evaluated, m is the age reduction factor dependent on the concrete mix proportions. According to Thomas' experiment [6], we employ

$$m = 0.2 + 0.4[FA/0.5] \tag{C.5}$$

The value of $D_{fc,ref}$ depends on the water to binder ratio w/b and the amount of fly ash FA of concrete. According to Petcherdchoo's [68], it can be given by

$$D_{fc,ref} = \frac{10^{[1.776+1.364(w/b)]} + [581 - 1869(w/b)][FA]}{3.1536 \times 10^{13}} \tag{C.6}$$

Appendix D. Moisture diffusion coefficient of non-carbonized concrete

The moisture diffusion coefficient of non-carbonized concrete D_h can also be calculated in terms of reference moisture diffusion coefficient $D_{h,ref}$ as follows

$$D_h = D_{h,ref}f_1(h)f_2(T)f_3(t_e) \tag{D.1}$$

where $f_1(h), f_2(T)$ and $f_3(t_e)$ are the influence functions of pore relative humidity, temperature and concrete aging respectively on moisture diffusion coefficient. They are given as

$$f_1(h) = \alpha_0 + \frac{1-\alpha_0}{1+[(1-h)/(1-h_c)]^n} \tag{D.2}$$

$$f_2(T) = \exp\left(\frac{U_m}{RT_{h,ref}} - \frac{U_m}{RT}\right) \tag{D.3}$$

$$f_3(t_e) = 0.3 + \sqrt{\frac{13}{t_e}} \tag{D.4}$$

where the value of α_0 is between 0.025 and 0.1, representing the ratio of min $D_{h,car}$ and max $D_{h,car}$. Here we take $\alpha_0 = 0.05$. $h_c = 0.75$ is the relative humidity at $D_{h,car}$ and drops halfway between the maximum and minimum values. The value of the exponent n is between 6 and 16, characterizing the spread of the drop in $D_{h,car}$. Here we take $n = 11$. $U_m \approx 20.3$ kJ/mol is the activation energy for hydration. $T_{h,ref} = 296$ K is the reference temperature.

References

[1] Z.P. Bažant, Physical model for steel corrosion in concrete sea structures-theory, J. Struct. Div. ASCE 105 (ST6) (1979) 1137–1153.
[2] J. Caims, State of the art report on bond of corroded reinforcement, Tech. report no. ceb-tg-2/5, ceb, 1998.
[3] D.W.S. Ho, R.K. Lewis, Carbonation of concrete and its prediction, Cem. Concr. Res. 17 (1987) 489–504.
[4] B. Hans (Ed.), Corrosion in Reinforced Concrete Structures, Woodhead Publishing Limited, England, 2005.
[5] C. Cao, M. Cheung, Non-uniform rust expansion for chloride-induced pitting corrosion in RC structures, Constr. Build. Mater. 51 (2014) 75–81.
[6] M.D.A. Thomas, P.B. Bamforth, Modelling chloride diffusion in concrete: effect of fly ash and slag, Cem. Concr. Res. 29 (4) (1999) 487–495.
[7] G. Glass, N. Buenfeld, The influence of chloride binding on the chloride induced corrosion risk in reinforced concrete, Corros. Sci. 42 (2) (2000) 329–344.
[8] C. Apostolopoulos, V. Papadakis, Consequences of steel corrosion on the ductility properties of reinforcement bar, Constr. Build. Mater. 22 (12) (2008) 2316–2324.
[9] C. Andrade, M. Prieto, P. Tanner, F. Tavares, R. d'Andrea, Testing and modelling chloride penetration into concrete, Constr. Build. Mater. 39 (2011) 9–18.
[10] C. Cao, 3D simulation of localized steel corrosion in chloride contaminated reinforced concrete, Constr. Build. Mater. 72 (2014) 434–443.
[11] A. Zanden, A. Taher, T. Arends, Modelling of water and chloride transport in concrete during yearly wetting/drying cycles, Constr. Build. Mater. 81 (2015) 120–129.
[12] L. Marsavina, K. Audenaert, G. Schutter, N. Faur, D. Marsavina, Experimental and numerical determination of the chloride penetration in cracked concrete, Constr. Build. Mater. 23 (1) (2009) 264–274.
[13] T. Ishida, P. Iqbal, H. Anh, Modeling of chloride diffusivity coupled with non-linear binding capacity in sound and cracked concrete, Cem. Concr. Res. 39 (10) (2009) 913–923.

[14] J. Ožbolt, G. Balabanic, G. Periskic, M. Kuster, Modelling the effect of damage on transport processes in concrete, Constr. Build. Mater. 24 (9) (2010) 1638–1648.
[15] B. Savija, J. Pacheco, E. Schlangen, Lattice modeling of chloride diffusion in sound and cracked concrete, Cem. Concr. Compos. 42 (2013) 30–40.
[16] M. Rahman, W. Al-Kutti, M. Shazali, M. Baluch, Simulation of chloride migration in compression-induced damage in concrete, J. Mater. Civil Eng. ASCE 24 (7) (2012) 789–796.
[17] R. Aveldano, N. Ortega, Behavior of concrete elements subjected to corrosion in their compressed or tensed reinforcement, Constr. Build. Mater. 38 (2013) 822–828.
[18] J. Ožbolt, G. Balabanic, M. Kuster, 3D numerical modelling of steel corrosion in concrete structures, Corros. Sci. 53 (12) (2011) 4166–4177.
[19] J. Ožbolt, F. Orsanic, G. Balabanic, M. Kuster, Modeling damage in concrete caused by corrosion of reinforcement: coupled 3D FE model, Int. J. Fract. 178 (1–2) (2012) 233–244.
[20] J. Ožbolt, F. Orsanic, G. Balabanic, Modeling pull-out resistance of corroded reinforcement in concrete: coupled three-dimensional finite element model, Cem. Concr. Compos. 46 (2014) 41–55.
[21] T. Huang, The experimental research on the interaction between concrete carbonation and chloride ingress under loading (Master thesis), Zhejiang University, 2013.
[22] P. Chindaprasirt, S. Rukzon, V. Sirivivatnanon, Effect of carbon dioxide on chloride penetration and chloride ion diffusion coefficient of blended portland cement mortar, Constr. Build. Mater. 22 (7) (2008) 1701–1707.
[23] X. Wan, F. Wittmann, T. Zhao, H. Fan, Chloride content and pH value in the pore solution of concrete under carbonation, J. Zhejiang Univ. Sci. A 4 (1) (2013) 71–78.
[24] M. Lee, S. Jung, B. Oh, Effects of carbonation on chloride penetration in concrete, ACI Mater. J. 110 (5) (2013) 559–566.
[25] I. Yoon, Deterioration of concrete due to combined reaction of carbonation and chloride penetration: experimental study, Key Eng. Mater. 348–349 (2007) 729–732.
[26] J. Backus, D. Mcpolin, M. Basheer, A. Long, N. Holmes, Exposure of mortars to cyclic chloride ingress and carbonation, Adv. Cem. Res. 25 (1) (2013) 3–11.
[27] P. Tumidajski, G. Chan, Effect of sulfate and carbon dioxide on chloride diffusivity, Cem. Concr. Res. 26 (4) (1996) 551–556.
[28] I. Yoon, Simple approach to calculate chloride diffusivity of concrete considering carbonation, Comput. Concr. 6 (1) (2009) 1–18.
[29] C. Yuan, D. Niu, D. Luo, Effect of carbonation on chloride diffusion in fly ash concrete, Comput. Concr. 5 (4) (2012) 312–316.
[30] A. Delnavaz, A. Ramezanianpour, The assessment of carbonation effect on chloride diffusion in concrete based on artificial neural network model, Mag. Concr. Res. 64 (10) (2012) 877–884.
[31] V. Ngala, C. Page, Effects of carbonation on pore structure and diffusional properties of hydrated cement pastes, Cem. Concr. Res. 27 (7) (1997) 995–1007.
[32] W. Puatatsananon, V. Saouma, Nonlinear coupling of carbonation and chloride diffusion in concrete, J. Mater. Civil Eng. ASCE 17 (3) (2005) 264–275.
[33] O. Isgor, A. Razaqpur, Finite element modeling of coupled heat transfer, moisture transport and carbonation processes in concrete structures, Cem. Concr. Compos. 26 (1) (2004) 57–73.
[34] A. Saetta, R. Vitaliani, Experimental investigation and numerical modeling of carbonation process in reinforced concrete structures part I: theoretical formulation, Cem. Concr. Res. 34 (4) (2004) 571–579.
[35] A. Saetta, R. Vitaliani, Experimental investigation and numerical modeling of carbonation process in reinforced concrete structures: Part II. Practical applications, Cem. Concr. Res. 35 (5) (2005) 958–967.
[36] V. Papadakis, C. Vayenas, M. Fardis, Fundamental modeling and experimental investigation of concrete carbonation, ACI Mater. J. 88 (4) (1991) 363–373.
[37] V. Papadakis, C. Vayenas, M. Fardis, A reaction engineering approach to the problem of concrete carbonation, J. Am. Inst. Chem. Eng. 35 (10) (1989) 1639–1650.
[38] V. Papadakis, C. Vayenas, M. Fardis, Physical and chemical characteristics affecting the durability of concrete, ACI Mater. J. 88 (2) (1991) 186–196.
[39] S. Brunauer, J. Skalny, E. Bodor, Adsorption on non-porous solids, J. Colloid Interface Sci. 30 (4) (1969) 546–552.
[40] A. Saetta, R. Scotta, R. Vitaliani, Mechanical behavior of concrete under physical–chemical attacks, J. Eng. Mech. ASCE 124 (10) (1998) 1100–1109.
[41] A. Neville, Properties of Concrete, Longman and John Wiley, London and New York, 1995.
[42] D. Niu, L. Chen, C. Zhang, Computational model of gas diffusion coefficient in concrete, J. Xian Univ. Arch. Technol. (Nat. Sci. Ed.) 39 (6) (2007) 741–745.
[43] C. Yuan, D. Niu, N. Chen, F. Duan, Influence of carbonation on the microstructure of concrete, Bull. Chin. Ceram. Soc. 32 (4) (2013) 687–691.
[44] E. Bastidas-Arteaga, A. Chateauneuf, M. Sanchez-Silva, P.H. Bressolette, F. Schoefs, A comprehensive probabilistic model of chloride ingress in unsaturated concrete, Eng. Struct. 33 (3) (2011) 720–730.
[45] K. Nakarai, T. Ishida, K. Maekawa, Multi-scale physicochemical modeling of soil-cementitious material interaction, Soils Found. 46 (5) (2006) 653–663.
[46] F. Duprat, N. Vu, A. Sellier, Accelerated carbonation tests for the probabilistic prediction of the durability of concrete structures, Constr. Build. Mater. 66 (2014) 597–605.
[47] A. Morandeau, M. Thiery, Dangla, Investigation of the carbonation mechanism of CH and C–S–H in terms of kinetics, microstructure changes and moisture properties, Cem. Concr. Res. 56 (2014) 153–170.
[48] E. Tolentino, F. Lanmeiras, A. Gomes, C. Silva, W. Vasconcelos, Effects of high temperature on the residual performance of portland cement concretes, Mater. Res. 5 (3) (2002) 301–307.
[49] E. Tolentino, F. Lanmeiras, A. Gomes, C. Silva, W. Vasconcelos, Structural evaluation and performance of portland cement concretes after exposure to high temperatures, Mater. Res. 5 (1) (2002) 27–36.
[50] Y. Kim, K. Lee, J. Bang, S. Kwon, Effect of w/c ratio on durability and porosity in cement mortar with constant cement amount, Adv. Mater. Sci. Eng. (2014) 1–11.
[51] Q. Zeng, K. Li, F. Teddy, P. Dangla, Pore structure characterization of cement pastes blended with high-volume fly-ash, Cem. Concr. Res. 42 (1) (2012) 194–204.
[52] J. Liu, Q. Qiu, F. Xing, D. Pan, Permeation properties and pore structure of surface layer of fly ash concrete, Materials 7 (6) (2014) 4282–4296.
[53] P. Chindaprasirt, C. Jaturapitakkul, T. Sinsiri, Effect of fly ash fineness on microstructure of blended cement paste, Constr. Build. Mater. 21 (7) (2013) 1534–1541.
[54] M. Thiery, P. Faure, A. Morandeau, G. Platret, J. Bouteloup, P. Belin, Effect of carbonation on the microstructure and moisture properties of cement-based materials, in: 12th International Conference on Building Materials and Components, Porto (Portugal), vol. 3, 2011, pp. 1–8.
[55] M. Thiery, V. Baroghel-Bouny, A. Morandeau, P. Dangla, Impact of Carbonation on the Microstructure and Transfer Properties of Cement-based Materials, Transfert, Ecole Centrale de Lille, 2012. pp. 1–10.
[56] T. Bier, J. Kropp, H. Hilsdorf, Carbonation and realcalinisation of concrete and hydrated cement paste, Durab. Constr. Mater. 3 (1987) 927–934.
[57] L. Tang, L. Nilsson, Chloride binding capacity and binding isotherms of opc pastes and mortars, Cem. Concr. Res. 23 (2) (1993) 247–253.
[58] G. Glass, N. Buenfeld, The influence of the chloride binding on the chloride induced corrosion risk in reinforced concrete, Corros. Sci. 42 (2) (2000) 329–344.
[59] A. Saetta, R. Scotta, R. Vitaliani, Analysis of chloride diffusion into partially saturated concrete, ACI Mater. J. 90 (5) (1993) 441–451.
[60] B. Martin-Perez, S. Pantazopoulou, M. Thomas, Numerical solution of mass transport equations in concrete structures, Comput. Struct. 79 (13) (2001) 1251–1264.
[61] Z. Bažant, L. Najjar, Nonlinear water diffusion in nonsaturated concrete, Mater. Struct. 5 (1) (1972) 546–552.
[62] Z. Bažant, L. Najjar, Drying of concrete as a nonlinear diffusion problem, Cem. Concr. Res. 1 (5) (1971) 461–473.
[63] L. Bertolini, B. Elsener, P. Pedeferri, E. Redaelli, R. Polder, Corrosion of Steel in Concrete – Prevention, Diagnosis, Repair, 2nd Edition., Wiley VCH, Weinheim, 2013.
[64] C. Page, N. Short, A.E. Tarras, Diffusion of chloride ions in hardened cement pastes, Cem. Concr. Res. 11 (3) (1981) 395–406.
[65] K.A.T. Vu, M.G. Stewart, Structural reliability of concrete bridges including improved chloride-induced corrosion models, Struct. Saf. 22 (4) (2000) 313–333.
[66] C. Yuan, D. Niu, G. Qi, Chloride ions diffusion performance of concrete under the combined effect of carbonation and salt spray, J. Jiangsu Univ. 34 (5) (2013) 605–609.
[67] Y. Xi, Z.P. Bažant, H. Jennings, Moisture diffusion in cementitious materials adsorption isotherms, Struct. Saf. 1 (6) (1994) 248–257.
[68] A. Petcherdchoo, Time dependent models of apparent diffusion coefficient and surface chloride for chloride transport in fly ash concrete, Constr. Build. Mater. 38 (8) (2013) 497–507.